Journal of Molecular Structure 1273 (2023) 134311

Contents lists available at ScienceDirect

Journal of Molecular Structure

journal homepage: www.elsevier.com/locate/molstr

Single-step approach for synthesis of a novel tetracyclic skeleton: Investigation of X-ray analysis, fluorescence spectra, TD-DFT calculations and biological activities

Burak Kuzu[a,b], Sergen Gül[a,b], Meltem Tan-Uygun[a,b], Mesude Figen Dönmez[c], Nurettin Menges[a,b,d,1,*]

[a] Pharmaceutical Chemistry Section, Van Yüzüncü Yil University, Tusba, Van, Turkey
[b] SAFF Chemical Reagent Research Laboratory, Van, Turkey
[c] Plant Protection Department, Faculty of Agriculture, Iğdir University, Iğdir, Turkey
[d] Science Technology Research and Application Center (BITAM), Necmettin Erbakan University, 42100, Köyceğiz-Konya, Turkey

ARTICLE INFO

Article history:
Received 16 July 2022
Revised 23 September 2022
Accepted 10 October 2022
Available online 11 October 2022

Keywords:
N-propargylated heterocycle
Imidazole
Single crystal
Fluorescence spectra
DFT calculation

ABSTRACT

Tetracyclic molecules show important properties such as biological activities and fluorescence sensors. Hence, in this study, we have reported unknown tetracyclic skeleton. *N*-propargylated C-2 and C-4 disubstituted imidazole derivatives were reacted by 2-aminomethyl piperidine without using any transition metal. The reaction unveiled 16 different imidazo[1,2-a]pyrido[1′,2′:3,4]imidazo[2,1-c]pyrazine skeletons. Cyclization reaction tolerated phenyl, naphthyl, bi-phenyl, 2-thienyl, and many substituents on the benzene ring such as OMe, CF_3, and halogens. We have uncovered the exact structure of the tetracyclic skeleton using single-crystal X-ray analysis. Significant fluorescence emission of tetracyclic molecules was investigated, and derivatives bearing electron-withdrawing groups, CF_3, and the 2-thienyl group possessed a bathochromic effect (shift to longer wavelength) which was confirmed by not only steady-state experiments but HOMOs and LUMOs calculations. The antimicrobial effects of the synthesized molecules on six different organisms were tested. Considerable activities of molecules **5p** and **5n** on many organisms were determined. Docking modeling and Lipinski, Ghose, and Veber compatibility studies of two different molecules were performed.

1. Introduction

Synthetic approaches to complex tetracyclic systems using efficient premeditated condensation or cyclization reactions among logically designed synthons are of considerable interest, as they provide quick, atom economical, and green chemistry access to compounds that may otherwise be difficult to obtain. For this reason, to reach polyheterocyclic compounds with simple starting materials would be highly welcomed, and this demand prompted us to establish such reactions for further applications. These reactions naturally create conceivably unlimited opportunities to combine various reactivity-matched synthons and individually explore either the heterocyclic core or the periphery of the compound. Tetracyclic molecules are widely under investigation due to their essential potentials such as agonist of GABAA α5 receptor [1], mirtazapine **2**, treatment of human immunodeficiency virus (HIV) [2], bis-alkylation reagent for DNA [3a], neonicotinoid insecticide **3** (Fig. 1A) [3b]. Tetracyclic benzimidazole molecule **4** was synthesized, and its antitumor effect was studied by Settimo and his research group (Fig. 1A) [3c]. Synthetic strategies in which synthesizing tetracyclic molecules was mentioned, include different pathways that cover multiple reaction steps [4a-c] or using nano- or transition metal-catalysts [5a-b]. However, we have explored a simplistic road to reach tetracyclic molecules in which sython molecules were undergone cyclization using 2-aminomethyl piperidine without any additives and catalyst. We have noticed that the discussed method and tetracyclic molecules were not reported yet. This study is, therefore, exhibiting both new synthetic ideas and a novel tetracyclic skeleton, which is named imidazo[1,2-a]pyrido[1′,2′:3,4]imidazo[2,1-c]pyrazine (Fig. 1B).

In our previous report, our research group revealed many synthetic methodologies for the different heterocyclic skeletons [6a-b,d]. In our previous studies, we have synthesized different cyclic product using *N*-propargylimidazole. One of those studies, we have shown that the reaction of *N*-propargylimidazole derivatives with piperidine leads to the form pyridine ring resulting in a benzannu-

* Corresponding author.
E-mail address: nurettin.menges@erbakan.edu.tr (N. Menges).
[1] www.saffchemical.com

https://doi.org/10.1016/j.molstruc.2022.134311
0022-2860/

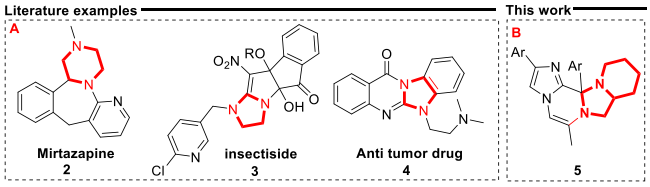

Fig. 1. Some important tetracyclic molecules and our synthesized skeleton.

Table 1
Optimum conditions for tetracyclic product.

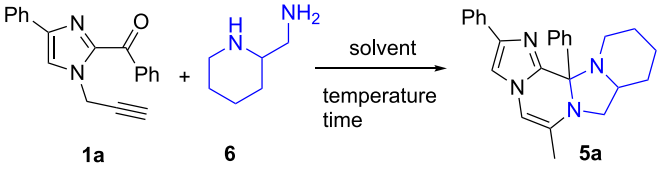

Entry	Solvent	Temperature (°C)	Time (h)	Yield for 5a
1	EtOH	78	12	–
2	THF	65	24	32
3	Benzene	80	24	38
4[a]	DMF	120	24	55
5[b]	DMF	150	24	61
6[c]	DMF	150	24	71
7[d]	DMF	150[e]	12	92
8	DMF	150	24	57

[a] compound **6** was used 1 fold;.
[b] compound **6** was used 3 fold;.
[c] compound **6** was used 5 fold;.
[d] compound **6** was used 5 fold, and the reaction was progressed in a sealed tube;.
[e] value indicates oil bath temperature.

lation product [6c], and we have envisaged that one amine group at the C-2 position of piperidine might give further intramolecular cyclization. Therefore, we have studied this theory and aspire to share the synthetic, fluorescence, TD-DFT and biological activity results in this paper.

2. Results and discussion

N-propargylimidazole derivatives, **1a-s**, were synthesized following our previous procedure [7]. These derivatives were then reacted with 2-aminomethyl piperidine under different reaction conditions in which solvent, temperature, and equivalent of amine were controlled. The polar protic solvent did not yield any cyclic product (Table 1, entry 1). However, THF (tetrahydrofuran) and benzene gave moderate yields (Table 1, entries 2–3). When we utilized DMF as a solvent, we saw an increase in the yield (Table 1, entry 4). Moreover, we have witnessed that the amount of compound **6** affects the yield of cyclic products (Table 1, entry 4–8). It is because of that compound **6** prompted the isomerization of the propargyl group to allene isomer, leading the cyclization [6c]. With a sealed tube, reaction time decreased, and the yield of the product increased up to 92%(Table 1, entry 7). Sealed tube gives a little amont of pressure which trigger the reaction to be completed in a [1]shorter time than traditional way. Final reaction conditions were revealed, as seen in Table 1, entry 7.

Characterization of compounds was concluded using 1D- and 2D-NMR. Furthermore, the structure of compound **5a** was authenticated by applying a single-crystal X-ray analysis (Fig. 2A-C) [8]. X-ray analysis attested that the aryl ring, which attaches to the newly formed chiral center, was perpendicular to the tetracyclic skeleton (Fig. 2C). X-ray data showed a hydrogen bond between the hydrogen atom of the C-2 position of the piperidine ring and the lone pair of the nitrogen atom of the imidazole ring, having a distance of 2.67 Å (Fig. 2B). In addition, bond angle of newly formed chiral center was found to be 101.5° (Fig. 2B). 3D figure of compound **5a** was shown in Fig. 2C.

The second track for the cyclization reaction was to search out the scope of the reaction. We have observed that cyclization reaction tolerated unsubstituted and some of the substituted benzene rings, naphthyl, biphenyl, and heteroaromatic rings. Unfortunately, we could not form compound 5 m and 5 s, which bears a nitro group at the para position of the benzene ring. We think that we can explain this situation with the nucleophilic aromatic substitution mechanism. This mechanism has been used for halogen-containing nitro benzene derivatives [9]. We have also reported six tetracyclic derivatives, possessing one substituent at the C-2 position of the imidazole ring (compounds **5h-i, 5n-5r** Scheme 1).

We have then proposed the reaction mechanism, as seen in Scheme 2. There are two possible reactions of the carbonyl group with secondary and primary amine units (A-1 or A-2). Further reaction, resulting in cyclization, is to attack a nitrogen atom to the polarized carbon atom (B). Basic media allows the isomerization of the propargyl unit to the allene (C) [10]. Middle carbon of the allene unit undergoes a nucleophilic attack by the nitrogen atom of the imidazolidine ring to create a tetracyclic ring system. This attack is an example of 6-exo-dig cyclization (D) [11]. Final step comprises hydrogen abstraction between quaternary nitrogen and carbanion atoms to stabilize the final product (E) [12].

Molecule **6** has a chiral center, and a new chiral center also appeared after the cyclization reaction. In this case, we have to say that the tetracyclic molecules should be formed as diastereomers. It is possible to say that two isomers are formed when some of NMR spectra showed more than chemical shifts. However, we could not succeed to obtain both isomers when purification was progressed. Selectivity towards one of diastereomers might be because of possible formation of imine intermediates (see A-1 and A-2). In both cases, steric hindrance might be the driving force for forming of thermodynamically favored imine intermediates which gives the reaction intermediate B (Scheme 2) [13]. It is hard to find out the exact diastereomer when NMR data was analysed. However, crystal structure (see Fig. 2C-D) gives details. When the 3D structure coming from the X-ray crystal is examined, it is seen that the unsubstituted benzene ring adjacent to the newly formed chiral center is perpendicular to the tetracyclic structure. When we look at the tetracyclic structure by taking benzene ring forward, it is seen that the proton, which is the neighbor of the chiral center in the piperidine ring, is also in front. In this position, the stereoisomer of both chiral centers was determined to be R,R. (see Scheme 2 stage E).

The purification of the molecules was carried out by column chromatography using the SiO_2 stationary phase. However, we have discerned that a new compound formed after chromatography, characterized as compound **7g**. One independent control experiment validated this result in which we have reacted compound **5g** with SiO_2 (Scheme 3) (See Scheme S1 for the assumed mechanism of ring-opening reaction). X-ray analysis of compound **5a** unveiled that the chiral center of the imidazolidine ring has a bond deviation in which the N–C-N bond angle was found to be 101.5° which should be 109.5° (See Fig. 7) [14]. This deviation might be making the ring more sensitive against ring opening to release ring tension through the driving force of any acidic media. We had then minimized the ratio of further ring-opening reaction when 3% triethylamine was added to the stationary phase of column chromatography.

Tetracyclic molecules have appeared as essential fluorescence features, such as fluorescent dyes [15a-b], fluorescent probe for DNA binding [15c-e], and fluorescent heterocycles for detecting

[1] There should be a reaction figure above the Table 1. I could not see it in proof version.

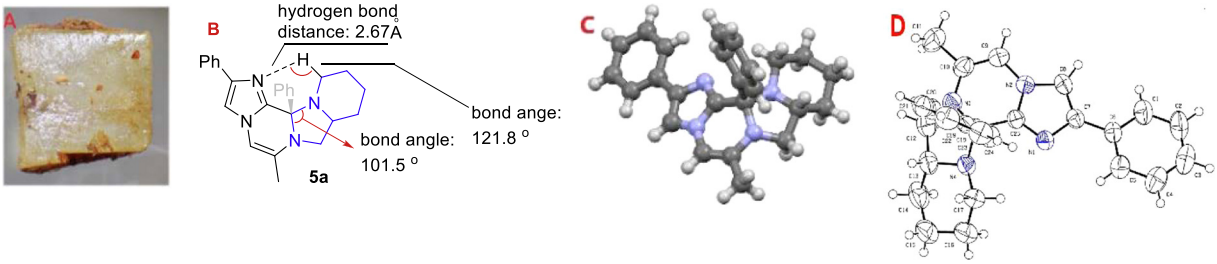

Fig. 2. **A** Photo of the single crystal for compound **5a** (taken under a microscope); **B**: 2D structure and some data for compound **5a; C**: 3D structure of compound **5a** from X-ray analysis (gray: carbon, blue: nitrogen, white: hydrogen). **D**: thermal ellipsoids for **5a**.

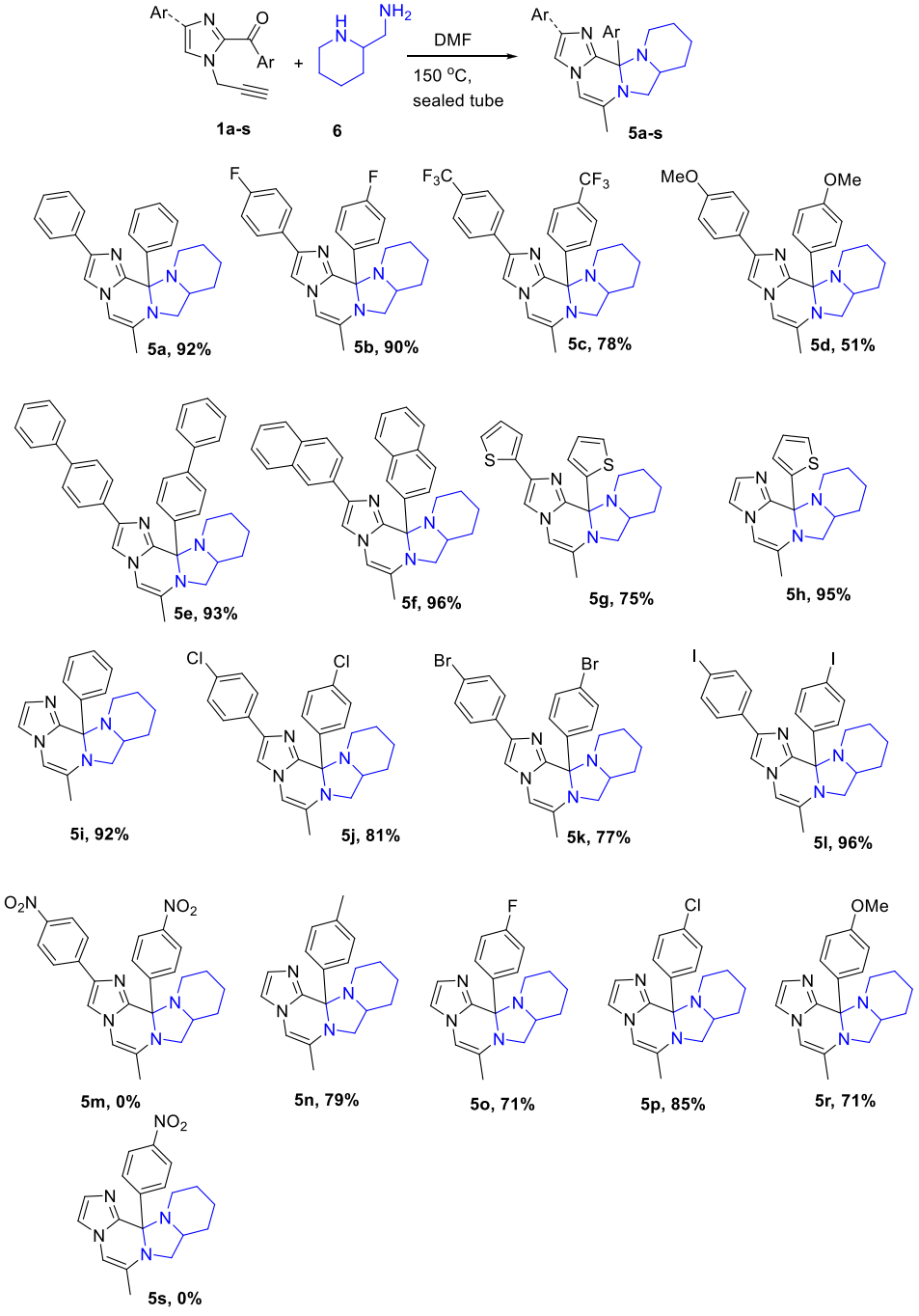

Scheme 1. Derivatives of tetracyclic compounds.

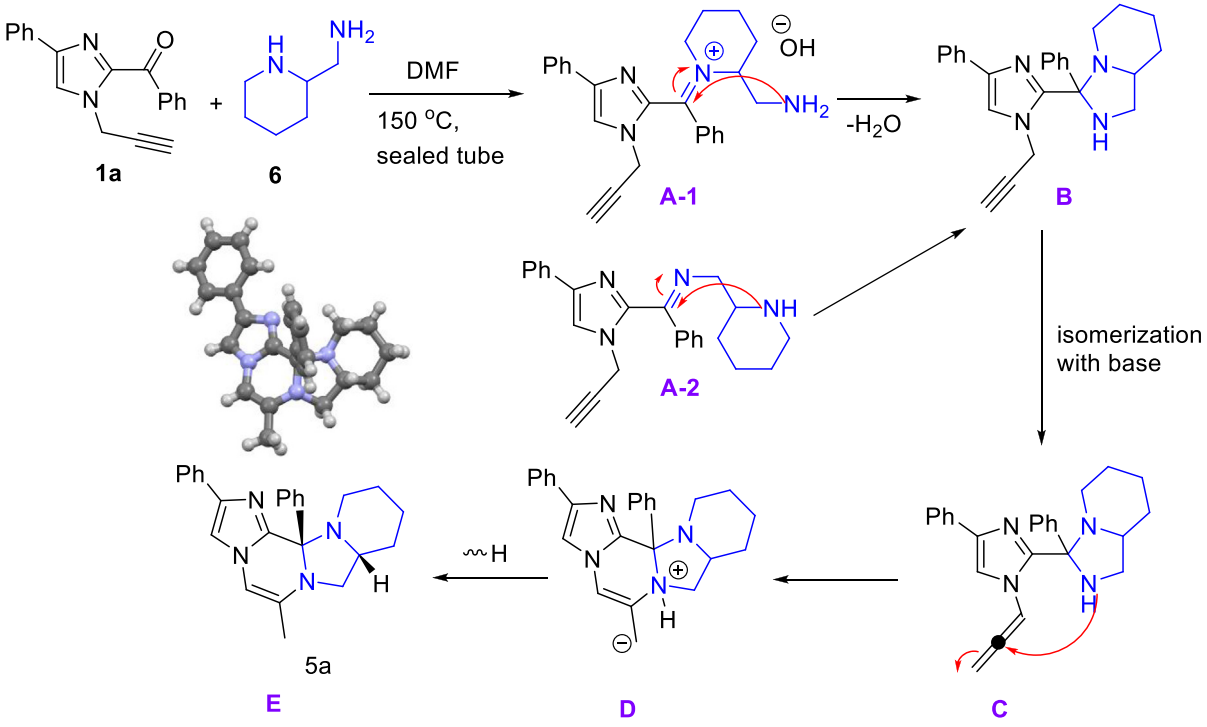

Scheme 2. The proposed reaction mechanism for tetracyclic molecules.

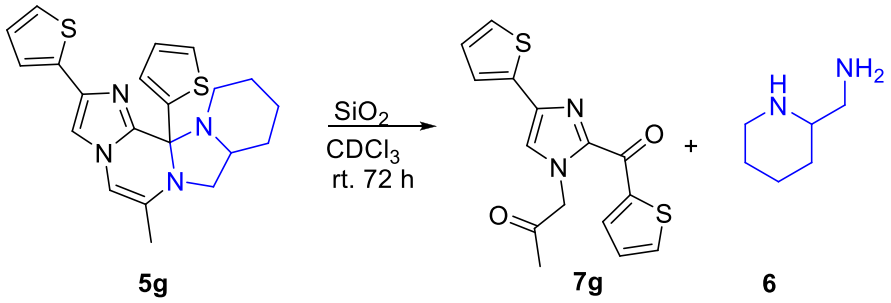

Scheme 3. Testing of reactivity of tetracyclic molecule against SiO_2.

the lysosome designed by Banerji, B [15f]. Due to the importance of further applications of tetracyclic molecules in the literature, we have measured fluorescence emission of synthesized tetracyclic molecules, and noteworthy fluorescence emissions were observed.

Synthesized molecules did not dissolve in water, and DMSO was chosen as the solvent. When the absorbances of the compound **5a-i** were examined, it was seen that there was no significant difference (between 288 and 382 nm), and generally, they had different absorbance levels at close wavelengths (Fig. 3). Important information was obtained by taking fluorescence emission measurements of the same molecules.

Fluorescence emission spectrum gave valuable results (Fig. 4, Table 2). For instance, compound **5a** displayed a weak fluorescence band at 429 nm. Compound **5e**, which bears biphenyl moiety, have a hypsochromic shift of about 37 nm, and did not show an emission at visible region (Table 2). Substituted derivative (Compound **5b**) was slightly bathochromically shifted up to 21 nm, as seen in Fig. 4. Compounds **5g** and **5h** showed an influence effect on the emission, which has a fluorescence band at 509 and 507 nm, respectively. However, their emission intensities are not valuable. An interesting information was obtained when the fluorescence potentials of the compounds **5a-i** were examined. The presence of a strong electron withdrawing group such as CF_3 (compound **5c)** in the para position of the benzene ring causes a bathochromic effect. The fluorescence intensity of this derivative is also favorable. On the other hand, the presence of a strong electron-withdrawing group such as OMe (Compound **5d**) in the same position causes the wavelength to be hypsochromically shifted. This derivative has higher fluorescence intensity. In addition, when analysis of compounds **5a-i,** the fluorescence emission of compounds **5i** and **5h** was observed as negligible.

Table 2
Absorbances and fluorescences of compound **5a-i**. Molecules were dissolved in DMSO with 50 μM.

Compound	$\lambda_{max.}$ (Absorbance, nm)	$\lambda_{max.}$ (Fluorescence, nm)
5a	288	429
5b	288 and 382	450
5c	288	498
5d	290	415
5e	296	392
5f	294	386
5 g	294 and 372	509
5h	288 and 300	507
5i	–	–

We tried to understand the important effect of electron donating and withdrawing groups on fluorescence emission by examining frontier orbitals. For this, we examined the HOMO and

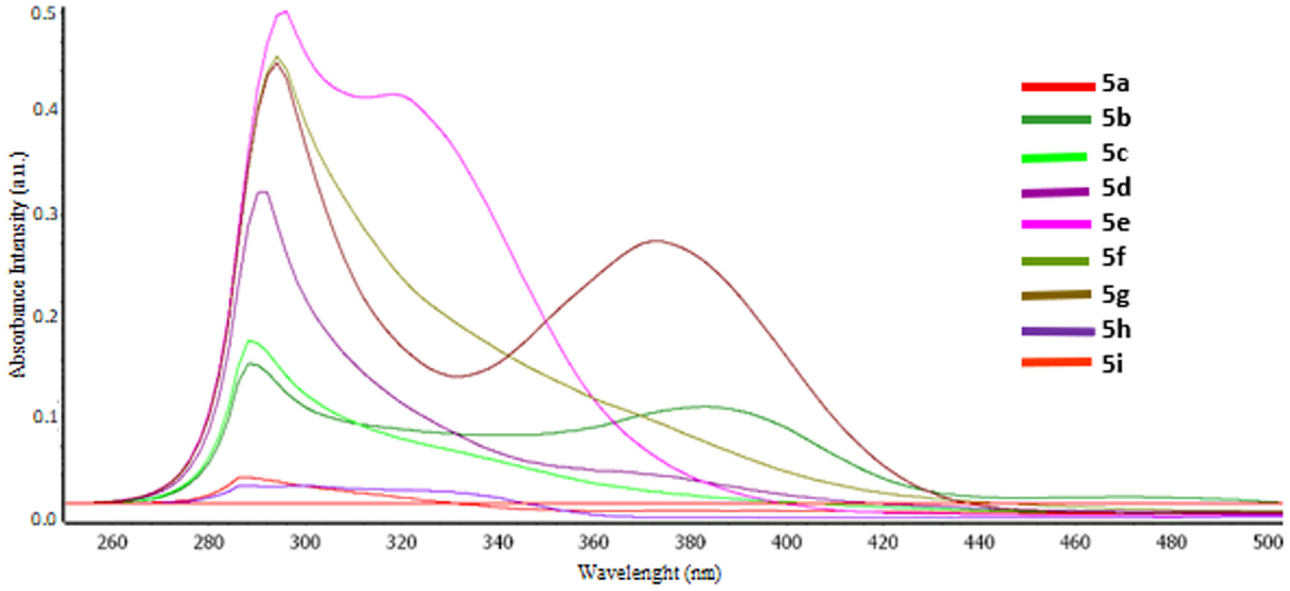

Fig. 3. Absorbance spectrum for compound **5a-i** in DMSO with 50 µM.

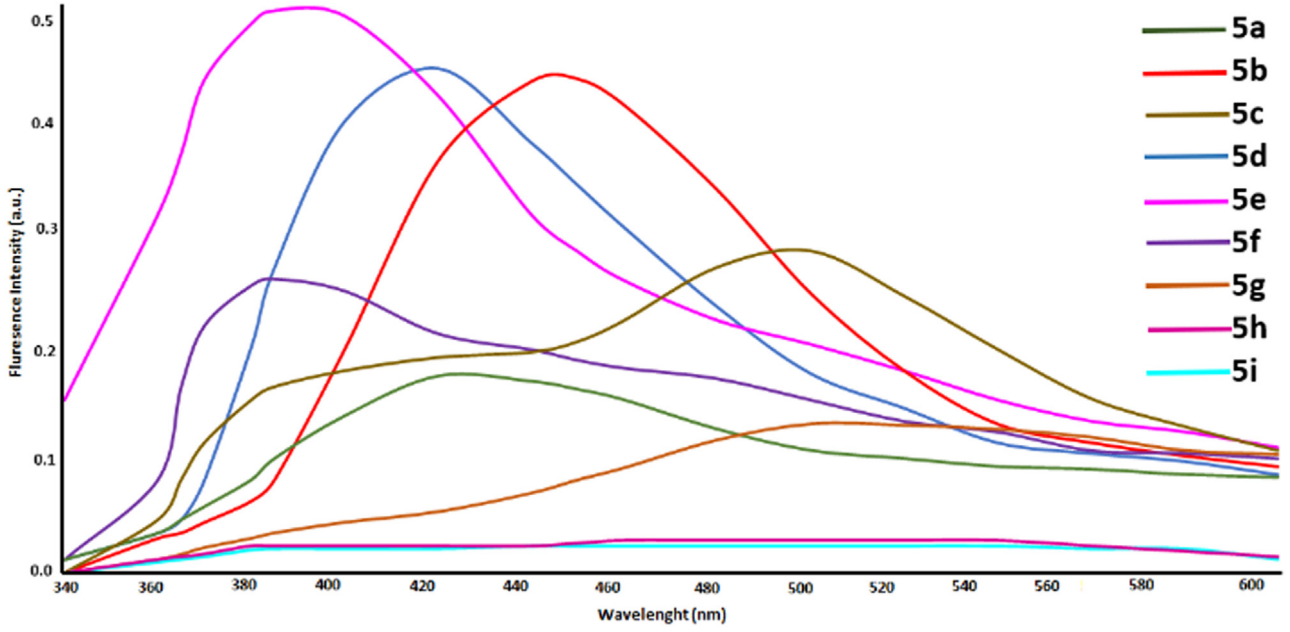

Fig. 4. Fluorescence spectrum for compound **5a-i** in DMSO with 50 µM. (λex at 336 nm, excitation, and emission slit widths = 4.5 nm)

LUMO orbitals of four different molecules. Unsubstituted benzene derivative (**5a**), molecule having electron withdrawing group (**5c**), molecule having electron donating group (**5d**), and molecule having heterocyclic ring (**5g**). For this reason, HOMOs and LUMOs of compounds **5a, 5c, 5d**, and **5g** were theoretically studied using TD-DFT calculations (Figure S1-S6) [16]. The HOMOs of compound **5a** (unsubstituted benzene) and **5d** (p-OMe-) are primarily localized at the tetracyclic unit and benzene ring, which is at C-4 position of the imidazole ring. LUMOs are almost in the same regions with almost no contribution from the benzene ring, which is perpendicular to the tetracyclic system. The distribution of frontier orbitals in similar regions for compound **5a** and **5d** (with some slight differences) is thought to show similar electronic effects in both molecules. This situation can be seen when looking at the emission bands of the **5a** and **5d** molecules. Molecule **5g** contains a heterocycle, unlike the benzene ring. This did not cause a remarkable difference in the HOMO and LUMO orbitals. However, the molecule **5g** has an emission band of 509 nm wavelength. This may be due to different transitions due to unshared electrons in the thiophene ring. It should be progressed detail experiments to support this idea. Differences between HOMOs and LUMOs of compound **5a** and **5g** are negligible. On the other hand, in the HOMOs of compound **5c** (p-CF_3-) and LUMOs of **5c** are located on the whole part of the aryl ring, perpendicular to the tetracyclic unit (Fig. 5), as opposed to other tetracyclic derivatives like **5a, 5d**, and **5g**. In this way, the presence of an electron withdrawing group on the para position of the benzene ring (**5c**) divided HOMOs and LUMOs into two separate regions, which might promote intramolecular charge transfer (ICT) [17]. Considering the TD-DFT calculations for the **5c** molecule, it was determined that the electronic transitions were intensely from HOMO to LUMO+1 and a lesser extent from HOMO to LUMO. Therefore, charge transfer from units of HOMOs to units

Table 3
Antimicrobial activities for synthesized molecules against different strains.*.

Strains	Conc.	Compounds															
		5a	5b	5c	5d	5e	5f	5 g	5h	5i	5j	5k	5l	5n	5o	5p	5r
Acine 177	NC	–	–	–	–	–	–	–	–	–	–	–	–	–	–	–	–
	PC	–	–	–	–	–	–	–	–	–	–	–	–	–	–	–	–
	25	–	–	–	–	–	–	–	–	–	–	–	–	–	–	–	–
	50	–	–	–	–	–	–	–	–	–	–	–	–	–	–	0.9	–
	100	–	–	–	–	–	–	–	0.6	–	–	–	–	–	–	1.0	–
E. coli 352	NC	–	–	–	–	–	–	–	–	–	–	–	–	–	–	–	–
	PC	–	1.5	1.5	1.5	1.5	1.5	1.5	1.5	1.5	1.5	1.5	1.5	1.5	1.5	1.5	1.5
	25	–	–	–	–	–	–	–	–	–	–	–	–	–	–	–	–
	50	–	–	0.6	–	–	–	–	–	–	–	–	–	–	–	–	–
	100	–	–	0.6	–	–	–	–	–	–	–	–	–	–	–	0.6	–
Entero 214	NC	–	–	–	–	–	–	–	–	–	–	–	–	–	–	–	–
	PC	2.0	2.0	2.0	2.0	2.0	2.0	2.0	2.0	2.0	2.0	2.0	2.0	2.0	2.0	2.0	2.0
	25	1.0	–	–	–	–	–	–	–	–	0.8	–	–	–	–	–	–
	50	1.0	–	–	–	–	–	0.6	–	–	1.0	–	–	1.2	–	2.0	–
	100	1.7	–	–	–	–	–	0.6	0.8	–	1.3	0.6	–	2.0	–	2.1	–
Mrsa 130	NC	–	–	–	–	–	–	–	–	–	–	–	–	–	–	–	–
	PC	1.5	1.5	1.5	1.5	1.5	1.5	1.5	1.5	1.5	1.5	1.5	1.5	1.5	1.5	1.5	1.5
	25	–	–	–	–	–	–	–	–	–	–	–	–	–	–	–	–
	50	–	–	–	–	–	–	–	–	–	–	–	–	–	–	1.0	–
	100	1.1	–	1.0	–	–	0.9	–	–	–	1.0	–	–	1.0	–	1.1	–
Mssa 272	NC	–	–	–	–	–	–	–	–	–	–	–	–	–	–	–	–
	PC	1.1	1.1	1.1	1.1	1.1	1.1	1.1	1.1	1.1	1.1	1.1	1.1	1.1	1.1	1.1	1.1
	25	–	–	–	–	–	0.7	–	–	–	–	–	–	–	–	–	–
	50	–	–	–	–	–	0.7	–	–	–	–	–	–	–	–	1.0	–
	100	1.1	–	1.0	–	–	0.7	–	–	–	1.0	–	–	1.1	–	1.0	–
Pae 250	NC	–	–	–	–	–	–	–	–	–	–	–	–	–	–	–	–
	PC	1.0	1.0	1.0	1.0	1.0	1.0	1.0	1.0	1.0	1.0	1.0	1.0	1.0	1.0	1.0	1.0
	25	–	–	–	–	–	–	–	–	–	–	–	–	–	–	–	–
	50	–	–	–	–	–	–	–	–	–	–	–	–	–	–	0.5	–
	100	–	–	0.6	–	–	–	–	–	–	–	–	–	–	–	0.7	–

* : To see name of strains, please look at experimental section. NC: Negative control, 10% DMSO; PC: Positive controle, Metilmicin.

Table 4
Docking scores after interaction of **5n, 5p** and tetracycline compounds with targets.

Entry	1HNW			2TRT		
	Binding Energy(kcal/mol)	Ligand efficiency	İnh. Const.(nM)	Binding Energy(kcal/mol)	Ligand efficiency	İnh. Const.(uM)
5n	−14.44	−0.60	26.04	−7.69	−0.32	2.3
5p	−14.62	−0.61	19.29	−7.84	−0.32	1.99
Tetracycline	−16.08	−0.50	1.62	−7.92	−0.25	1.56

of LUMOs for **5c** might be observed upon photoexcitation having a bathochromic effect, supported by steady-state experiments seen in Table 2.

2.1. Biological activities and computational modelling

The activities of the synthesized molecules on 6 different microorganisms were tested by disk diffusion technique. The results are given in Table 3 using three different concentrations.

According to the microbial tests, it was observed that the molecules did not have a serious effect against the selected strains in general. However, it would be appropriate to state that some molecules show activity similar or close to positive control against some species. It was observed that at least one molecule in Mssa 272 and entero 214 strains showed the same effect as the positive control. The most active molecules were found to be **5a** and **5n** for Mssa 272, while **5n** and **5p** for entero 214. As a result, it can be said that the molecule **5p**, which has an effect in all species, contains parachlorine substituent, and it can be said that the **5j** molecule, which is its close derivative, also shows valuable activity.

The synthesized molecules have a tetracyclic core. We are aware that an aromatic ring in the structure of our molecule stands perpendicular to the tetracyclic structure, contrary to the tetracycline structure used in the clinic, but we have calculated docking model of the two most suitable molecules to test the possibility of binding to the proteins affected by the antimicrobial agent expressed as tetracyclines. In the validation of the molecular docking study with the determined target structures, the tetracycline co-ligand was removed from the x-ray structure obtained from the protein database and re-docked. It was determined that the cluster RMSD values of the co-ligand molecule tested with 10 different conformations were ≤2A° for both pdb ID: 1HNW and pdb ID: 2TRT. Dcoking score was shown in Table 4.

The docking results of the molecules show that they give values close to the positive control. For this reason, it can be said that these molecules may have a possibility to act with a similar mechanism. We also showed which amino acids the positive control and **5n** and **5p** molecules bind to in the active site. On the other hand, it was observed in both protein structures that the molecules could not make the hydrogen bonds that the positive control did. When we look at the tetracycline structure, it is seen that there are many acceptor groups that can make hydro-

Table 5
Residues of 5n, 5p and tetracycline compounds interacting with targets.

	1HNW		2TRT	
Compounds	H-bonding	Other non-covalent interactions	H-bonding	Other non-covalent interactions
5n	–	**A965**, G966, C967, G1061, C1195, G1197,	–	His64, Phe86, Hıs100, Gln116, Ile134, Ser138
5p	–	G966, A968, C1195, G1197		His64, Phe86, His100, **Pro105, Ile134, Mg223**
Tetracycline	G966, C967, C1195, U1196, G1197, G1198	**A965**, G1198, Mg1631	Asn82, Thr103, Arg104, Gln116	Ser67, **Pro105**, Ile134, **Mg223**

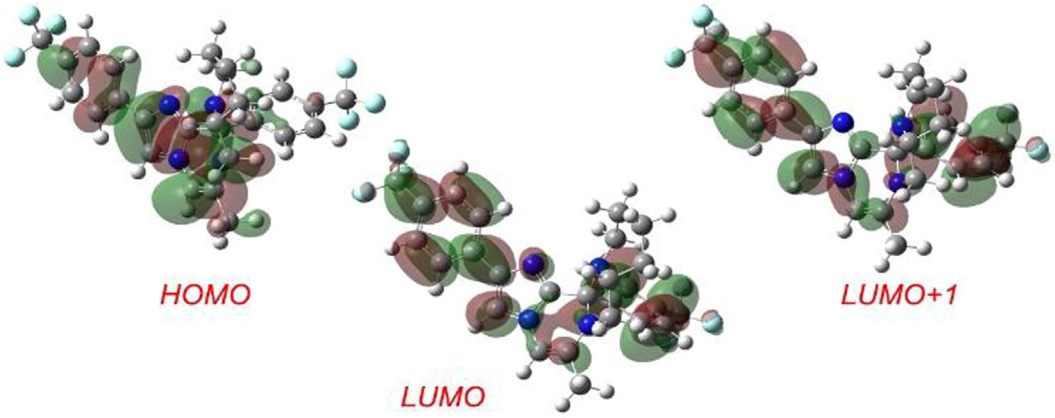

Fig. 5. TD-DFT calculation results for compound 5c.

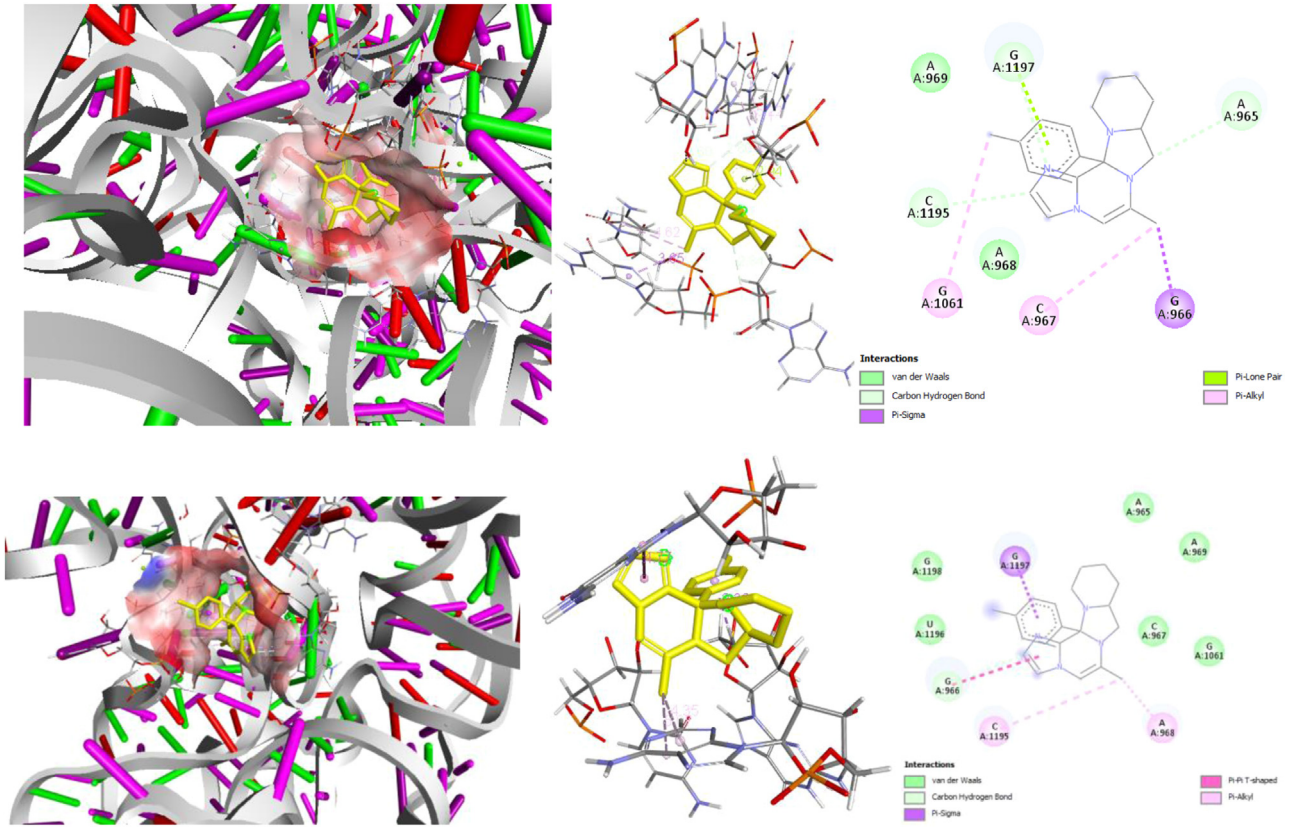

Fig. 6. Up images: complex for 1HNW-5n; down images: complex for 1HNW-5p

gen bonds (Table 5). We would like to express that the selected molecules also constitute preliminary information for further studies.

The positions of the molecules with amino acid residues in the active site for both selected proteins are also shown in the Figs. 6-7.

Finally, we calculated the basic physicochemical parameters of the molecules to test their compliance with the Lipinski, Ghose and Veber rules. We have determined that **5n** and **5p**, which were determined as the most suitable molecules according to the activity studies, comply with the Lipinski, Ghose and Veber criteria (Table 6).

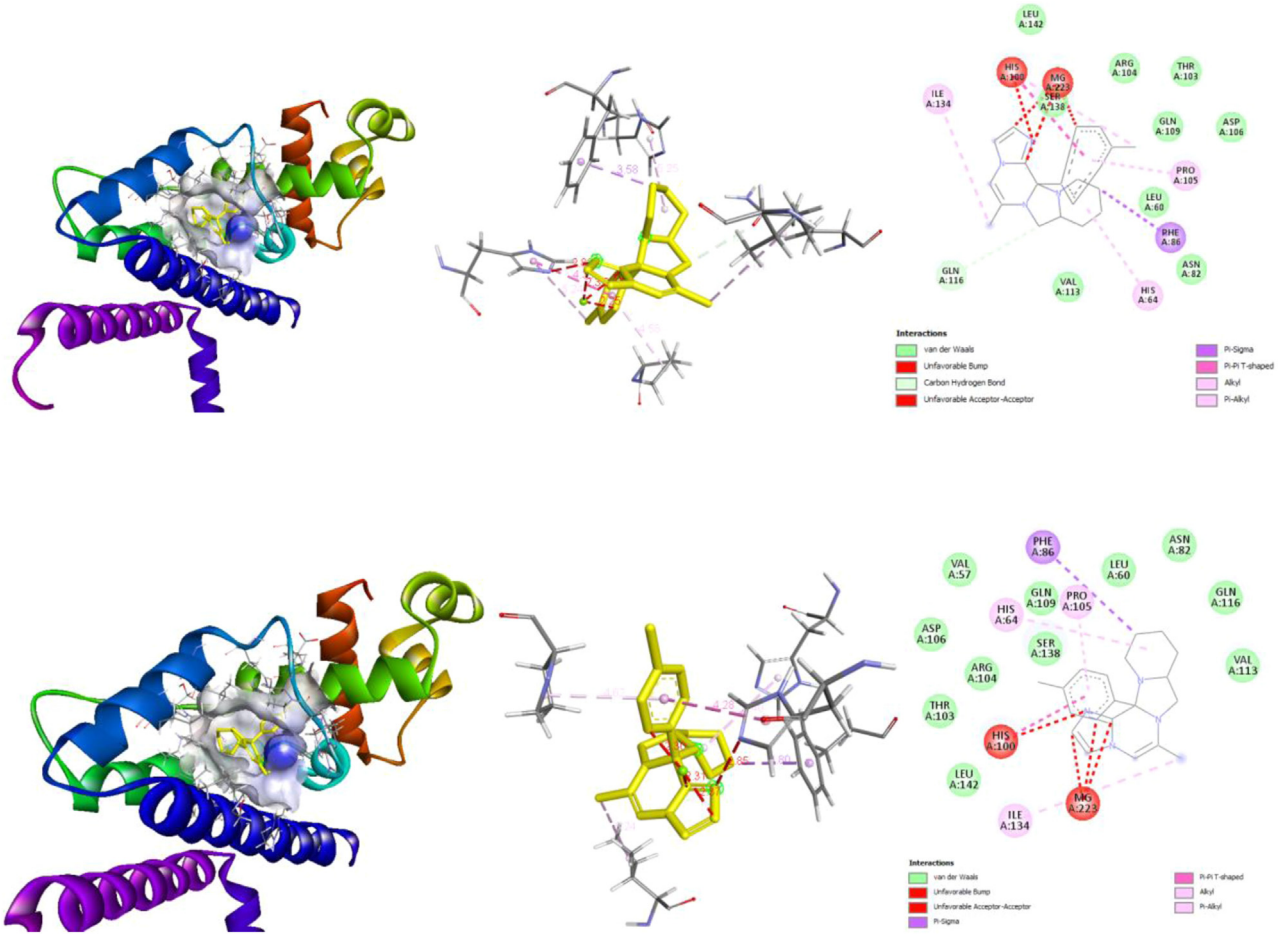

Fig. 7. Up images: complex for 2TRT-5n; down images: complex for 2TRT-5p

Table 6
Some druglikeness parameters of the synthesized compounds.

Compounds	MW (g/mol)	cLogP	HBA/HBD	Lipinski	Ghose	Veber
5a	382.50	4.868	4/0	Yes	Yes	Yes
5b	418.48	5.184	6/0	No	Yes	Yes
5c	518.19	6.71	8/0	No	No	Yes
5d	442.55	4.615	4/0	Yes	No	Yes
5e	534.69	8.218	2/0	No	No	Yes
5f	482.62	6.862	2/0	No	No	Yes
5 g	394.56	4.831	2/0	Yes	Yes	Yes
5h	312.43	2.75	2/0	Yes	Yes	Yes
5i	306.40	2.77	2/0	Yes	Yes	Yes
5j	450.138	5.984	2/0	No	No	Yes
5k	538.037	6.525	2/0	No	No	Yes
5l	634.29	7.582	2/0	No	No	Yes
5n	320.43	3.256	2/0	Yes	Yes	Yes
5o	324.40	2.927	3/0	Yes	Yes	Yes
5p	340.85	3.327	2/0	Yes	Yes	Yes
5r	336.43	2.642	3/0	Yes	Yes	Yes

MW: molecular weight; cLogP: calculated via ChemDraw software; HBA: Number of H-bond acceptors; HBD: Number of H-bond donors; Lipinski: mw≤500, logP ≤5, number of N or O≤ 10, number of NH or OH ≤5; Ghose: 160 ≤mw ≤480, 0 ≤logP ≤5.6, 40 ≤Molecular Refractivity ≤130, 20 ≤Atoms ≤70; Veber: Rotatable bonds ≤10, Total polar surface area ≤140.

3. Conclusion

In conclusion, we have designed an applicable synthetic protocol for a novel tetracyclic skeleton in which it was not used any additive or transition metal. By using different electronic and steric hindrance features, 16 different tetracyclic molecules were yielded. Tetracyclic derivatives were characterized both by NMR and X-ray analysis. Some bond deviation data was abstracted from X-ray analysis, which helps us predict tetracyclic molecules' reactivity. Synthesized tetracyclic molecules have two chiral centers which of them was formed after cyclization resulting in diastereomers. Some of the tetracyclic molecules displayed applicable fluorescence emission in which we have emerged the effect of electron-withdrawing group on bathochromic shifting. Thienyl substituted derivatives also showed bathocromically shifting up to 80 nm. Synthesized tetracyclic molecules and their uncovered electronic features might make tetracyclic molecules good candidates for fluorescent probes. The antimicrobial properties of the molecules were tested against six different derivatives. It is foreseen that molecules **5n** and **5p** can be considered as the beginning of further studies. In particular, the **5p** molecule was found to have activity in all selected organisms, in some of which it had equivalent activity to the positive control. Since the structures of the molecules are similar to tetracyclines, docking studies between the protein targeted by tetracyclines and molecules **5n** and **5p** were performed. While interaction with similar amino acid residues was obtained, it was observed that the hydrogen bond acceptors or donors required in the synthesized molecules should be designed if tetracyclice-liked activity is desired. Finally, by calculating the physicochemical parameters in terms of their potential to be lead compounds, it was determined that **5n** and **5p** molecules, which can be used as precursor compounds in future research, have appropriate parameters.This information can be an inspiration to find a more effective candidate for further studies.

4. Experimental section

4.1. General materials and method

The NMR spectra were recorded on Agilent-400 (400 MHz for ^{1}H NMR and 100 MHz for ^{13}C NMR) with $CDCl_3$ as the solvent and TMS as an internal reference. ^{1}H NMR spectral data was reported as follows: chemical shift (δ, ppm), multiplicity, integration, and coupling constants (Hz). ^{13}C NMR spectral data were reported in terms of the chemical shift. The following abbreviations were used to indicate multiplicities: s = singlet; d = doublet; t = triplet; q = quartet; m = multiplet. High-resolution mass spectra were obtained on a Thermo LC-MS/MS spectrometer in ESI mode and reported as m/z. UV absorbances and fluorescence measurements were done using BMG-Clariostar. Melting points were obtained on a X-4 digital melting point apparatus without correction. Purification of products was accomplished by column chromatography packed with silica gel. All reagents were purchased and used without further purification except for DMF, which was dried distillation method using P_2O_5 as a desiccant. All *N*-propargylated compounds, **1a-s**, were synthesized by the following procedure in our previous report [7].

4.2. Material method for X-ray analysis and single crystal

X-ray crystallographic analysis was completed by Bruker APEXII Quazar Diffractometer, Oxford 700 Low Temperature Device, and Zeiss CL-150 Microscop equipments, operated at Gebze Technical University.

A colorless block-like specimen of $C_{25}H_{26}N_4$ (compound **5a**), approximate dimensions 0.096 mm x 0.130 mm x 0.233 mm, was used for the X-ray crystallographic analysis. A total of 1240 frames were collected. The total exposure time was 3.44 h. The frames were integrated with the Bruker SAINT software package using a wide-frame algorithm. The integration of the data using a triclinic unit cell yielded a total of 9929 reflections to a maximum θ angle of 25.00° (0.84 Å resolution), of which 3504 were independent (average redundancy 2.834, completeness = 97.1%, Rint = 4.74%, Rsig = 5.57%) and 2146 (61.24%) were greater than 2σ(F2). The final cell constants of a= 8.4315(11) Å, b= 10.5847(14) Å, c= 12.0926(15) Å, α = 76.164(9)°, β = 79.881(9)°, γ = 83.485(11)°, volume = 1028.7(2) Å3, are based upon the refinement of the XYZ-centroids of 1231 reflections above 20 σ(I) with 4.921° < 2θ < 40.92° Data were corrected for absorption effects using the multi-scan method (SADABS). The ratio of minimum to maximum apparent transmission was 0.849. The calculated minimum and maximum transmission coefficients (based on crystal size) are 0.9830 and 0.9930.

The structure was solved and refined using the Bruker SHELXTL V6.14 Software Package, using the space group P −1, with Z= 2 for the formula unit, compound **5a**. The final anisotropic full-matrix least-squares refinement on F^2 with 263 variables converged at R1 = 5.38%, for the observed data and wR2 = 15.43% for all data. The goodness-of-fit was 1.046. The largest peak in the final difference electron density synthesis was 0.147 e-/Å3 and the largest hole was −0.282 e-/Å3 with an RMS deviation of 0.040 e-/Å3. On the basis of the final model, the calculated density was 1.235g/cm^3 and F(000), 408 e-.

100 mg compound **5a** was dissolved in EtOAc (10 mL). The solution was transferred to a beaker (50 mL) and the beaker was sealed with aluminum foil. Holes were drilled in several places of the foils and left for a week. The resulting crystal was separated from the solvent and dried at room temperature to prepare for analysis.

4.3. Synthesis

4.3.1. General procedure for cyclization

N-propargylated imidazole derivative (1 mmol) **1a-s** was dissolved in dry DMF (4 mL). 2-Methyl-aminopiperidine (**6**) (5 mmol) was added to the reaction tube. The tube was sealed and heated at 150 °C in an oil bath for 12 hrs. The reaction was controlled by TLC and terminated. The reaction media was poured into a flask, which included ice water. After ten minutes, precipitated occurred. Precipitated was filtered off with a filter funnel (No:4) and dried at room temperature. The crude product was purified by column chromatography with SiO_2-TEA (TEA; 3% w/v). **Preparing of basic silica**: 25g of silica gel was vigorously shaken with trimethylamine (1 mL) for 10 mins., and the mixture was used as a stationary phase for purification. Eluent for the mobile phase of chromatography: hexane:ethylacetate (10:1)

4.3.2. Control experiment for the ring-opening

Compound 5g (50 mg) was dissolved in $CDCl_3$ (1 mL), and 0.5g of SiO_2 was added to the reaction flask. The reaction flask was stirred at room temperature for 72 h. TLC control was indicated to terminate the reaction in which the starting material was not consumed totally. Reaction media was analyzed by ^{1}H NMR.

4.3.3. Biological activity and computational methods

Initial dilution with 10% dimethylsulfoxide (DMSO) solution as 1/1 v/v dilutions (100, 50, 25, mg/μl) were prepared. Nutrient Agar medium was used for the cultivation of bacterial strains. Then 10 μl of different concentrations of the substance released into the environment. The treated petri dishes are kept in an incubator set at 28 °C for bacterial growth. After 24 h, the zone of inhibition of pathogen growth was measured in cm. *Acinetobacter baumannii* MTBB 120,177 (Acine 177), *Escherichia coli* MTBB 100,352 (E.coli 352), *Staphylococcus aureus* MTBB 150,130 (Mrsa 130), *Staphylococcus aureus* MTBB 150,272 (Mssa 272), *Enretococcus* sp. MTBB110214 (Entero 214), *Pseudomonas aeruginosa* MTBB 130,250 (Pae 250) strains were tested. Antimicrobial tests were completed by Mesude Figen DÖNMEZ (Ph.D.) at Iğdır University.

Molecular docking studies were performed using AutoDock 4.2 software to determine the interactions of the synthesized tetracyclic compounds and the reference antibiotic drug Tetracycline with the structure of the thermus thermophilus 30 s ribosomal subunit in complex with tetracycline and tetracycline repressor class d structure. 3D crystal structures PDB ID:1HNW [18a] and PDB ID:2TRT [18b], respectively, were obtained from the RCSB Protein Data Bank (www.rcsb.org). The molecular structure of the compounds was drawn using Gaussview 5.0 and then optimized using the DFT method with the help of the Gaussian 09 package based on the theoretical level of the B3LYP method and the 6–31g basis set [16]. In molecular docking studies x: 205,835; y: 110.603; z: 4.277 for PDB ID:1HNW, and x: 22.225; y: 35,163; z: 34.573 for PDB ID: 2TRT were determined as coordinate centers. Then, using a grid box with 50 × 50 × 50 points at the center of the predicted locations and a grid point spacing of 0.375 Å, the lowest placed conformations were selected for further studies. Water molecules were removed with AutoDock tools and subsequently, polar hydrogen atoms, Gasteiger partial charges, and Kollman charges were added to the targets. Additionally, the rotatable bonds of the compounds were adjusted. Lamarckian genetic algorithm approach was applied in both simulations. The interactions of both targets with compounds were analyzed using the Discovery Studio Client 4.1 program.

4.4. Spectral data

4.4.1. 6-methyl-2,13a-diphenyl-8,8a,9,10,11,12-hexahydro-13aH imidazo[1,2a]pyrido[1′,2′:3,4]imidazo[2,1-c]pyrazine (5a)

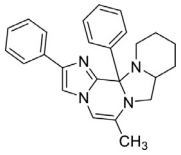

245 mg, 92% yield, transparent crystal, m.p. 234 °C, ^{1}H NMR (400 MHz, $CDCl_3$) δ (ppm) = 7.77–7.74 (m, 2H, Ar-H), 7.74 (s, 1H, Ar-H), 7.39–7.27 (m, 6H, Ar-H), 7.24–7.16 (m, 2H, Ar-H), 6.09 (quasi q, J = 1.1 Hz, 1H, -CH=C), 3.98–3.90 (m, 2H), 3.12–3.07 (m, 1H), 1.99 (d, J = 1.1 Hz, 3H, -CH_3), 1.85–1.79 (m, 1H), 1.68–1.62 (m, 2H), 1.58–1.49 (m, 2H), 1.30–1.21 (m, 2H), 1.06–0.98 (m, 1H). ^{13}C NMR (100 MHz, d_6-DMSO) δ (ppm) = 141.6, 140.1, 138.4, 134.9, 129.0, 128.9, 128.1, 127.9, 127.8, 126.6, 124.7, 110.4, 97.9, 79.3, 56.7, 52.8, 47.6, 28.9, 25.6, 23.6, 16.9. HRMS (ESI, m/z) calculated for $C_{25}H_{28}N_4$ $(M + 2H)^+$: 384.2314, Found: 384.2272.

4.4.2. 2,13a-bis(4-fluorophenyl)−6-methyl-8,8a,9,10,11,12-hexahydro-13aH-imidazo[1,2-a]pyrido[1′,2′:3,4]imidazo[2,1-c]pyrazine (5b)

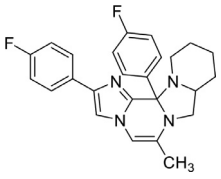

235 mg, 90% yield, dark red solid, m.p: 119–120 °C, ^{1}H NMR (400 MHz, $CDCl_3$) δ (ppm)= 7.80–7.75 (m, AA'BB' system, 2H, Ar-H), 7.45–7.40 (m, AA'BB' system, 2H, Ar-H), 7.06–7.04 (m, AA'BB' system, 2H, Ar-H), 7.00–6.96 (m, AA'BB' system, 2H, Ar-H), 6.93 (s, 1H, Ar-H), 5.87 (quasi q, J = 1.2 Hz, 1H, N–CH=C), 4.11–4.06 (m, 1H), 3.86 (dd, J = 6.3 Hz, J = 7.7 Hz, 1H), 3.22 (dd, J = 7.8 Hz, J = 9.9 Hz, 1H), 2.65–2.58 (m, 1H), 2.00 (d, J = 1.2 Hz, 3H, -CH_3), 1.91–1.81 (m, 2H), 1.77–1.73 (m, 2H), 1.53–1.47 (m, 1H), 0.91–0.82 (m, 2H). ^{13}C NMR (100 MHz, $CDCl_3$) δ (ppm)= 162.2 (d, J = 246.5 Hz), 161.7 (d, J = 244.3 Hz), 141.5, 140.6, 133.8 (d, J = 2.9 Hz), 131.0 (d, J = 3.1 Hz), 129.6 (d, J = 8.0 Hz), 128.1, 126.4 (d, J = 7.8 Hz), 115.1 (d, J = 21.4 Hz), 114.4 (d, J = 21.2 Hz), 109.0, 98.4, 79.1, 56.8, 53.1, 47.8, 28.6, 25.1, 23.4, 17.0. HRMS (ESI, m/z) calculated $C_{25}H_{25}F_2N_4$ $(M + H)^+$: 419.2047, Found:419.2051.

4.4.3. 6-methyl-2,13a-bis(4-(trifluoromethyl)phenyl)−8,8a,9,10,11,12-hexahydro-13aH-imidazo[1,2-a]pyrido[1′,2′:3,4]imidazo[2,1-c]pyrazine (5c)

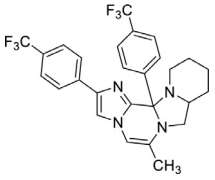

192 mg, 78% yield, light green solid, m.p: 86–87 °C, ^{1}H NMR (400 MHz, $CDCl_3$) δ (ppm)=7.94–7.89 (m, AA'BB' system, 2H, Ar-H), 7.61–7.58 (m, AA'BB' system, 2H, Ar-H), 7.57 (bs, 4H, Ar-H), 7.09 (s, 1H, Ar-H), 5.91 (quasi q, J = 1.2 Hz, 1H, -CH=C), 4.15–4.09 (m, 1H), 3.91 (dd, J = 6.3 Hz, J = 7.8 Hz, 1H), 3.26 (dd, J = 7.8 Hz, J = 9.9 Hz, 1H), 2.66–2.60 (m, 1H), 2.03 (d, J = 1.2 Hz, 3H, -CH_3), 1.90–1.84 (m, 2H), 1.77–1.74 (m, 2H), 1.54–1.45 (m, 1H), 0.89–0.83 (m, 2H). ^{13}C NMR (100 MHz, $CDCl_3$) δ (ppm) = 141.9, 141.4, 140.2, 138.1, 129.2, 128.6, 128.2, 127.8 (J = 271 Hz, F_3_C), 127.6 (J = 271 Hz, F_3_C), 125.3 (q, J = 3.9 Hz), 124.8, 124.7 (q, J = 3.9 Hz), 111.1, 110.6, 98.4, 79.2, 56.9, 53.1, 47.8, 28.6, 25.1, 23.3, 17.0. HRMS (ESI, m/z) calculated for $C_{27}H_{25}F_6N_4$ $(M + H)^+$: 519.1983, Found: 519.1979

4.4.4. 2,13a-bis(4-methoxyphenyl)−6-methyl-8,8a,9,10,11,12-hexahydro-13aH-imidazo[1,2-a]pyrido[1′,2′:3,4]imidazo[2,1-c]pyrazine (5d)

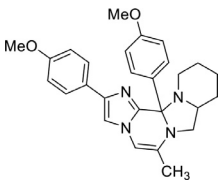

131 mg, 51% yield, light yellow solid, m.p: 89–92 °C, ^{1}H NMR (400 MHz, $CDCl_3$) δ (ppm) = 7.77–7.73 (m, AA'BB' system, 2H, Ar-H), 7.38–7.35 (m, AA'BB' system, 2H, Ar-H), 6.92–6.89 (m, AA'BB' system, 2H, Ar-H), 6.88 (s, 1H, Ar-H), 6.84–6.80 (m, AA'BB' system, 2H, Ar-H), 5.85 (quasi q, J = 0.8 Hz, 1H, -CH=C), 4.14–4.08 (m, 1H), 3.91–3.89 (m, 1H), 3.82 (s, 3H, OMe), 3.76 (s, 3H, OMe), 3.22 (d, J = 7.8 Hz, J = 9.8 Hz, 1H), 2.67–2.61 (m, 1H), 1.98 (d, J = 0.8 Hz, 3H, -CH_3), 1.86–1.78 (m, 2H), 1.76–1.69 (m, 2H), 1.51–1.47 (m, 1H), 0.90–0.85 (m, 2H). ^{13}C NMR (100 MHz, $CDCl_3$) δ (ppm) = 158.9, 158.3, 141.6, 141.1, 129.2, 128.1, 127.8, 126.1, 113.8, 112.9, 108.3, 98.4, 79.2, 56.8, 55.3, 55.1, 53.0, 47.8, 29.7, 28.7, 25.1, 23.5, 17.0. HRMS (ESI, m/z) calculated for $C_{27}H_{31}N_4O_2$ $(M + H)^+$: 443.2447, Found:443.2450.

4.4.5. 2,13a-di([1,1′-biphenyl]−4-yl)−6-methyl-8,8a,9,10,11,12-hexahydro-13aH-imidazo[1,2-a]pyrido[1′,2′:3,4]imidazo[2,1-c]pyrazine (5e)

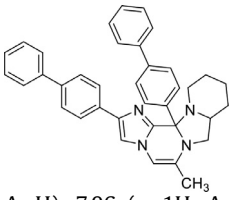

226 mg, 93% yield, dark red solid, m.p. 178–179 °C, ^{1}H NMR (400 MHz, $CDCl_3$) δ (ppm) = 7.95–7.92 (m, AA'BB' system, 2H, Ar-H), 7.67–7.64 (m, 2H, Ar-H), 7.63–7.61 (m, AA'BB' system, 2H, Ar-h), 7.59–7.56 (m, 2H, Ar-H), 7.54 (bs, 3H, Ar-H), 7.48 −7.44 (m, 3H, Ar-H), 7.43–7.39 (m, 2H, Ar-H), 7.36–7.31 (m, 2H, Ar-H), 7.06 (s, 1H, Ar-H), 5.92 (quasi q, J = 1.1 Hz, 1H,-CH=C), 4.26–4.19 (m, 1H), 3.93 (dd, J = 6.4 Hz, J = 7.6 Hz, 1H), 3.29 (dd, J = 7.8 Hz, J = 9.8 Hz, 1H), 2.78–2.69 (m, 1H), 2.04 (d, J = 1.1 Hz, 3H, -CH_3), 1.92–1.86 (m, 2H), 1.80–1.72 (m, 2H), 1.57–1.50 (m, 1H), 0.91–0.85 (m, 2H). ^{13}C NMR (100 MHz, $CDCl_3$) δ (ppm) = 141.8, 141.5, 135.8, 133.9, 132.8, 132.7, 132.5, 128.5, 128.0, 127.8, 127.5, 127.1, 126.6, 126.4, 126.0, 125.8, 124.9, 124.1, 122.8, 110.0, 98.4, 79.8, 57.0, 53.1, 48.0, 28.7, 25.2, 23.4, 17.1. HRMS (ESI, m/z) calculated for $C_{37}H_{36}N_4$ $(M + 2H)^+$: 536.2940, Found:536.2903.

4.4.6. 6-methyl-2,13a-di(naphthalen-2-yl)−8,8a,9,10,11,12-hexahydro-13aH-imidazo[1,2-a]pyrido[1′,2′:3,4]imidazo[2,1-c]pyrazine (5f)

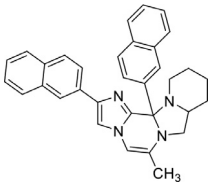

241 mg, 95% yield, light yellow solid, m.p: 183–185 °C, ^{1}H NMR (400 MHz, $CDCl_3$) δ (ppm) =8.35 (bs, 1H, Ar-H), 8.00–7.96 (m, 1H, Ar-H), 7.95–7.88 (m, 2H, Ar-H), 7.87–7.78 (m, 5H, Ar-H), 7.76 (d, J = 1.2 Hz, 2H, Ar-H), 7.47–7.41 (m, 3H, Ar-H), 7.13 (s, 1H, Ar-H), 5.92 (d, J = 1.2 Hz, 1H, -CH=C), 4.01–4.00 (m, 1H), 4.00 (dd, J = 6.4 Hz, J = 7.6 Hz, 1H), 3.32 (dd, J = 7.8 Hz, J = 9.8 Hz, 1H), 2.82–2.80 (m, 1H), 2.08 (d, J = 1.2 Hz, 3H, -CH_3), 1.90–1.84 (m, 2H), 1.78–1.71 (m, 2H), 1.57–1.53 (m, 1H), 0.94–0.84 (m, 2H). ^{13}C NMR (100 MHz, $CDCl_3$) δ (ppm) = 141.6, 141.3, 141.1, 140.7, 140.3, 138.9, 137.1, 134.1, 128.7, 128.6, 128.4, 128.2, 127.2, 127.0, 126.9, 126.8, 126.3, 125.3, 109.6, 98.4, 79.5, 56.9, 53.1, 47.9, 28.8, 25.2, 23.5, 17.0. HRMS (ESI, m/z) calculated for $C_{33}H_{31}N_4$ $(M + H)^+$: 483.2549, Found:483.2556.

4.4.7. 6-methyl-2,13a-di(thiophen-2-yl)−8,8a,9,10,11,12-hexahydro-13aH-imidazo[1,2-a]pyrido[1′,2′:3,4]imidazo[2,1-c]pyrazine (5g)

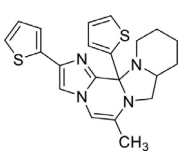

199 mg, 75% yield, dark red solid, m.p: 149–150 °C, ^{1}H NMR (400 MHz, $CDCl_3$) δ (ppm) =7.27–7.25 (m, 1H, Ty-H), 7.21 (dd, J = 1.5 Hz, J = 4.8 Hz, 1H, Ty-H), 7.13 (dd, J = 1.0 Hz, J = 5.1 Hz, 1H, Ty-H), 7.00 (dd, J = 3.5 Hz, J = 5.1 Hz, 1H, Ty-H), 6.97–6.93 (m, 2H, Ty-H), 6.89 (s, 1H, Ar-H), 5.90 (bs, 1H, -CH=C), 4.13–4.07 (m, 1H), 3.81–3.78 (m, 1H), 3.10–3.06 (m, 1H), 2.87–2.80 (m, 1H), 1.94 (bs, 3H, -CH_3), 1.80–1.71 (m, 3H), 1.53–1.41 (m, 2H), 1.19–1.15 (m,1H), 0.90–0.82 (m, 1H). ^{13}C NMR (100 MHz, $CDCl_3$) δ (ppm) = 144.8, 141.5, 138.7, 136.6, 128.3, 127.5, 127.2, 126.9, 125.0, 122.7, 121.7, 109.0, 99.2, 57.1, 53.2, 47.6, 28.6, 25.1, 23.5, 17.0. HRMS (ESI, m/z) calculated for $C_{21}H_{23}N_4S_2$ $(M + H)^+$: 395.1364, Found:395.1369.

4.4.8. 6-methyl-13a-(thiophen-2-yl)−8,8a,9,10,11,12-hexahydro-13aH-imidazo[1,2-a]pyrido[1′,2′:3,4]imidazo[2,1-c]pyrazine (5h)

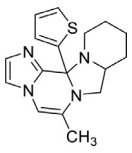

277 mg, 95% yield, light yellow solid, m.p: 160–162 °C, ^{1}H NMR (400 MHz, $CDCl_3$) δ (ppm) = 7.20 (dd, J = 1.2 Hz, J = 5.0 Hz, 1H,Ty-H), 7.06 (d, J = 1.3 Hz, 1H, Ar-H), 6.94 (dd, J = 3.6 Hz, J = 5.0 Hz, 1H, Ty-H), 6.83 (dd, J = 1.2 Hz, J = 3.6 Hz, 1H, Ty-H), 6.71 (d, J = 1.3 Hz, 1H, Ar-H), 5.93 (q, J = 1.2 Hz, 1H, -CH=C), 3.94 (m, 1H), 3.78 (dd, J = 5.9 Hz, J = 7.4 Hz, 1H), 3.04 (dd, J = 7.4 Hz, J = 9.9 Hz, 1H), 2.87–2.80 (m, 1H), 1.93 (d, J = 1.2 Hz, 3H, -CH_3), 1.89–1.83 (m, 2H), 1.79–1.73 (m, 2H), 1.47–1.42 (m, 1H), 0.92–0.80 (m, 2H). ^{13}C NMR (100 MHz, $CDCl_3$) δ (ppm)= 145.3, 141.6, 128.5, 128.1, 127.4, 126.4, 125.0, 113.7, 99.8, 77.2, 57.3, 53.2, 47.9, 28.7, 25.1, 23.5, 16.9. HRMS (ESI, m/z) calculated for $C_{17}H_{21}N_4S$ $(M + H)^+$: 313.1487, Found:313.1486.

4.4.9. 6-methyl-13a-phenyl-8,8a,9,10,11,12-hexahydro-13aH-imidazo[1,2-a]pyrido[1′,2′:3,4]imidazo[2,1-c]pyrazine (5i)

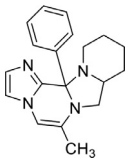

270 mg, 92%, white solid, m.p: 164–165 °C, ^{1}H NMR (400 MHz, $CDCl_3$) δ (ppm) = 7.38–7.35 (m, 2H, Ar-H), 7.30–7.25 (m, 2H, Ar-H), 7.22–7.18 (m, 1H, Ar-H), 7.07 (d, J = 1.3 Hz, 1H, Ar-H), 6.68 (d, J = 1.3 Hz, 1H, Ar-H), 5.83 (quasi q, J = 1.2 Hz, 1H, -CH=C), 3.91–3.87 (m, 1H), 3.84 (dd, J = 6.3 Hz, J = 7.7 Hz, 1H), 3.17 (dd, J = 7.7 Hz, J = 9.9 Hz, 1H), 2.69–2.61 (m, 1H), 1.96 (d, J = 1.2 Hz, 3H, -CH_3), 1.87–1.77 (m, 2H), 1.74–1.68 (m, 2H), 1.49–1.39 (m, 1H), 0.89–0.80 (m, 2H). ^{13}C NMR (100 MHz, $CDCl_3$) δ (ppm) = 141.4, 138.4, 128.4, 128.0, 127.6, 127.5, 127.5, 113.7, 98.8, 79.7, 57.1, 53.0, 48.1, 28.7, 25.2, 23.4, 16.9. HRMS (ESI, m/z) calculated for $C_{19}H_{23}N_4$ $(M + H)^+$: 307.1923, Found:307.1924.

4.4.10. 2,13a-bis(4-chlorophenyl)−6-methyl-8,8a,9,10,11,12-hexahydro-13aH-imidazo[1,2-a]pyrido[1′,2′:3,4]imidazo[2,1-c]pyrazine (5j)

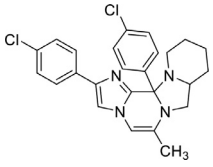

207 mg, 81% yield, light brown solid, m.p: 141–142 °C, ^{1}H NMR (400 MHz, $CDCl_3$) δ (ppm) = 7.76–7.73 (m, AA'BB' system, 2H, Ar-H), 7.39–7.36 (m, AA'BB' system, 2H, Ar-H), 7.32–7.29 (m, AA'BB' system, 2H, Ar-H), 7.27–7.25 (m, AA'BB' system, 2H, Ar-H), 6.98 (s, 1H, Ar-H), 5.87 (d, J = 1.1 Hz, 1H, -CH=C), 4.11–4.07 (m, 1H), 3.86 (dd, J = 6.3 Hz, J = 7.7 Hz, 1H), 3.22 (dd, J = 7.8 Hz, J = 9.9 Hz, 1H), 2.65–2.57 (m, 1H), 2.00 (d, J = 1.1 Hz, 3H, -CH_3), 1.88–1.83 (m, 2H), 1.78–1.73 (m, 2H), 1.52–1.47 (m, 1H), 0.90–0.84 (m, 2H). ^{13}C NMR (100 MHz, $CDCl_3$) δ (ppm) = 141.4, 140.4, 136.5, 133.6, 133.3, 131.7, 129.3, 128.4, 128.3, 127.8, 126.1, 109.6, 98.4, 79.1, 56.8, 53.1, 47.7, 28.6, 25.1, 23.3, 17.0. HRMS (ESI, m/z) calculated for $C_{25}H_{25}Cl_2N_4$ $(M + H)^+$: 451.1456, Found: 451.1463.

4.4.11. 2,13a-bis(4-bromophenyl)−6-methyl-8,8a,9,10,11,12-hexahydro-13aH-imidazo[1,2-a]pyrido[1′,2′:3,4]imidazo[2,1-c]pyrazine (5k)

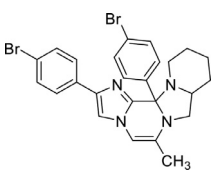

118 mg, 77% yield, dark brown solid, m.p: 92–95 °C, ^{1}H NMR (400 MHz, $CDCl_3$) δ (ppm) = 7.70–7.67 (m, AA'BB' system, 2H, Ar-H), 7.47–7.44 (m, AA'BB' system, 2H, Ar-H), 7.44–7.41 (m, AA'BB' system, 2H, Ar-H), 7.34–7.30 (m, AA'BB' system, 2H, Ar-H), 6.97 (s, 1H, Ar-H), 5.86 (quasi q, J = 1.2 Hz, 1H,-CH=C), 4.11–4.04 (m, 1H), 3.84 (dd, J = 6.3 Hz, J = 7.7 Hz, 1H), 3.21 (dd, J = 7.8 Hz, J = 9.9 Hz, 1H), 2.64–2.57 (m, 1H), 1.99 (d, J = 1.2 Hz, 3H, -CH_3), 1.87–1.83 (m, 2H), 1.77–1.72 (m, 2H), 1.52–1.44 (m, 1H), 0.99–0.88 (m, 2H). ^{13}C NMR (100 MHz, $CDCl_3$) δ (ppm) = 141.4, 140.4, 137.1, 133.8, 131.4, 130.8, 129.6, 128.3, 126.5, 121.9, 119.8, 109.7, 98.4, 79.2, 56.8, 53.1, 47.8, 28.6, 25.1, 23.4, 17.0. HRMS (ESI, m/z) calculated for $C_{25}H_{25}Br_2N_4$ $(M + H)^+$: 541.0426, Found:541.0457.

4.4.12. 2,13a-bis(4-iodophenyl)−6-methyl-8,8a,9,10,11,12-hexahydro-13aH-imidazo[1,2-a]pyrido[1′,2′:3,4]imidazo[2,1-c]pyrazine (5l)

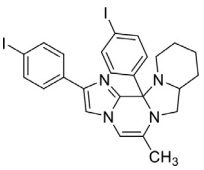

227 mg, 95% yield, red solid, m.p: 127–128 °C, ^{1}H NMR (400 MHz, $CDCl_3$) δ (ppm) = 7.67–7.64 (m, AA'BB' system, 2H, Ar-H), 7.63–7.60 (m, AA'BB' system, 2H, Ar-H), 7.57–7.54 (m, AA'BB' system, 2H, Ar-H), 7.19–7.16 (m, AA'BB' system, 2H, Ar-H), 6.99 (s, 1H, Ar-H), 5.86 (quasi q, J = 1.2 Hz, 1H,-CH=C), 4.10–4.04 (m, 1H), 3.84 (dd, J = 6.3 Hz, J = 7.7 Hz, 1H), 3.21 (dd, J = 7.8 Hz, J = 9.9 Hz, 1H), 2.64–2.56 (m, 1H), 1.99 (d, J = 1.2 Hz, 3H, -CH_3), 1.89–1.80 (m, 2H), 1.79–1.73 (m, 2H), 1.53–1.44 (m, 1H), 0.91–0.84 (m, 2H). ^{13}C NMR (100 MHz, $CDCl_3$) δ (ppm) = 141.3, 140.4, 137.7, 137.3, 136.8, 134.4, 129.9, 128.3, 126.8, 109.7, 98.4, 93.9, 91.1, 79.3, 56.8, 53.1, 47.7, 28.6, 25.1, 23.3, 17.0. HRMS (ESI, m/z) calculated for $C_{25}H_{25}I_2N_4$ $(M + H)^+$: 635.0169, Found: 635.0181.

4.4.13. 6-methyl-13a-(p-tolyl)−8,8a,9,10,11,12-hexahydro-13aH-imidazo[1,2-a]pyrido[1′,2′:3,4]imidazo[2,1-c]pyrazine (5n)

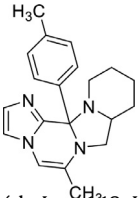

210 mg, 79% yield, brown solid, m.p: 151–152 °C,^{1}H NMR (400 MHz, $CDCl_3$) δ (ppm) =7.27–7.24 (m, AA'BB' system, 2H, Ar-H), 7.12–7.09 (m, AA'BB' system, 2H, Ar-H), 7.07 (d, J = 1.26 Hz, 1H, Ar-H), 6.69 (d, J = 1.26 Hz, 1H, Ar-H), 5.84 (quasi q, J = 1.18 Hz, 1H), 3.89–3.83 (m, 2H), 3.18 (dd, J = 7.72 Hz, J = 9.86 Hz, 1H), 2.70–2.62 (m, 1H), 2.29 (s, 3H, Ar-CH_3), 1.97 (d, J = 1.18 Hz, 3H, -CH_3), 1.84–1.81 (m, 1H), 1.75–1.69 (m, 3H), 1.66–1.60 (m, 1H), 1.50–1.41 (m, 1H), 1.11–1.04 (m, 1H). ^{13}C NMR (100 MHz, $CDCl_3$) δ (ppm) = 141.6, 137.2, 135.3, 128.4, 128.0, 127.6, 127.1, 113.7, 98.7, 57.2, 52.9, 48.1, 28.7, 25.2, 23.5, 21.0, 16.9. HRMS (ESI, m/z) calculated for $C_{20}H_{24}N_4$ $(M + K)^+$: 359.1638, Found: 359.1635.

4.4.14. 13a-(4-fluorophenyl)−6-methyl-8,8a,9,10,11,12-hexahydro-13aH-imidazo[1,2-a]pyrido[1′,2′:3,4]imidazo[2,1-c]pyrazine (5o)

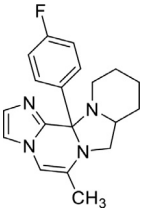

195 mg, 71% yield, brown solid, m.p: 107–108 °C, ^{1}H NMR (400 MHz, $CDCl_3$) δ (ppm) = 7.38–7.33 (m, AA'BB' system, 2H, Ar-H), 7.08 (d, J = 1.25 Hz, 1H, Ar-H), 6.99–6.95 (m, AA'BB' system, 2H, Ar-H), 6.72 (d, J = 1.25 Hz, 1H, Ar-H), 5.88 (quasi q, J = 1.18 Hz, 1H), 3.86–3.82 (m, 2H), 3.18 (dd, J = 7.75 Hz, J = 9.94 Hz, 1H), 2.66–2.59 (m, 1H), 1.98 (d, J = 1.18 Hz, 3H, -CH_3), 1.85–1.82 (m, 1H), 1.75–1.68 (m, 3H), 1.50–1.41 (m, 1H), 1.14–1.08 (m, 1H). ^{13}C NMR (100 MHz, $CDCl_3$) δ (ppm) = 163.4, 161.0, 129.4 (d, J = 8.1 Hz), 128.5, 128.0, 114.4 (d, J = 21.2 Hz), 113.8, 98.9, 57.1, 53.0, 48.0, 28.6, 25.2, 23.4, 17.0. HRMS (ESI, m/z) calculated for $C_{19}H_{21}FN_4$ $(M + H)^+$: 325.1828, Found: 325.1823.

4.4.15. 13a-(4-chlorophenyl)−6-methyl-8,8a,9,10,11,12-hexahydro-13aH-imidazo[1,2-a]pyrido[1′,2′:3,4]imidazo[2,1-c]pyrazine (5p)

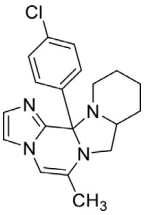

202 mg, 85% yield, dark brown solid, m.p: 146 °C, ^{1}H NMR (400 MHz, $CDCl_3$) δ (ppm) =7.33–7.30 (m, AA'BB' system, 2H, Ar-H), 7.27–7.23 (m, AA'BB' system, 2H, Ar-H), 7.07 (d, J = 1.27 Hz, 1H, Ar-H), 6.71 (d, J = 1.27 Hz, 1H, Ar-H), 5.87 (quasi q, J = 1.20 Hz, 1H), 3.85–3.80 (m, 2H), 3.17 (dd, J = 7.76 Hz, J = 9.93 Hz, 1H), 2.65–2.58 (m, 1H), 1.97 (d, J = 1.20 Hz, 3H, -CH_3), 1.74–1.61 (m, 4H), 1.49–1.39 (m, 1H), 1.15–1.06 (m, 1H). ^{13}C NMR (100 MHz, $CDCl_3$) δ (ppm) = 141.1, 137.0,

133.5, 129.1, 128.5, 128.0, 127.8, 113.8, 99.0, 57.1, 53.0, 28.6, 48.0, 28.6, 25.2, 23.3, 17.0. HRMS (ESI, *m/z*) calculated for $C_{19}H_{21}ClN_4$ $(M + H)^+$: 341.1533, Found: 341.1524.

4.4.16. 13a-(4-methoxyphenyl)−6-methyl-8,8a,9,10,11,12-hexahydro-13aH-imidazo[1,2-a]pyrido[1′,2′:3,4]imidazo[2,1-c]pyrazine (5r)

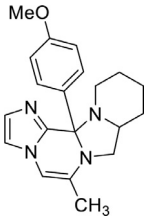

188 mg, 71% yield, white solid, m.p: 104–105 °C, ^{1}H NMR (400 MHz, $CDCl_3$) δ (ppm) = 8.49–8.48 (m, 1H, Ar-H), 7.91–7.82 (m, AA'BB' system, 2H, Ar-H), 7.54–7.34 (bs, 2H, Ar-H), 6.91–6.82 (m, AA'BB' system, 2H, Ar-H), 3.81 (s, 3H, -OMe), 3.78–3.69 (m, 1H), 3.58–3.48 (m, 1H), 3.32–3.21 (m, 1H), 3.18–3.07 (m, 1H), 2.75–2.64 (m, 1H), 1.90 (s, 3H, -CH_3), 1.86–1.75 (m, 2H), 1.75–1.42 (m, 4H). ^{13}C NMR (100 MHz, $CDCl_3$) δ (ppm) = 167.6, 162.2, 129.3, 126.2, 113.5, 56.6, 55.3, 44.5, 42.7, 27.1, 23.9, 22.9, 22.6. HRMS (ESI, *m/z*) calculated for $C_{20}H_{24}N_4O$ $(M + H)^+$: 337.2028, Found: 337.2022.

4.4.17. 1-(4-(thiophen-2-yl)−2-(thiophene-2-carbonyl)−1H-imidazol-1-yl)propan-2-one (7g)

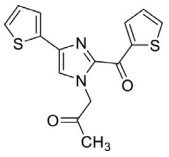

^{1}H NMR (400 MHz, $CDCl_3$) δ =8.64 (dd, J = 1.2 Hz, J = 3.9 Hz, 1H, Ty-H), 7.74 (dd, J = 1.2 Hz, J = 4.9 Hz, 1H, Ty-H), 7.37 (dd, J = 1.2 Hz, J = 3.6 Hz, 1H, Ty-H), 7.27 (dd, J = 1.2 Hz, J = 5.1 Hz, 1H, Ty-H), 7.23 (s, 1H, Ar-H), 7.19 (dd, J = 3.9 Hz, J = 4.9 Hz, 1H, Ty-H), 7.07 (dd, J = 3.6 Hz, J = 5.1 Hz, 1H, Ty-H), 5.24 (s, 2H, -CH_2-), 2.33 (s, 3H, -CH_3). ^{13}C NMR (100 MHz, $CDCl_3$) δ=199.9, 174.7, 141.4, 141.2, 137.4, 136.9, 136.6, 135.9, 128.1, 127.6, 124.5, 123.2, 121.9, 57.7, 27.2. HRMS (ESI, *m/z*) calculated for $C_{15}H_{13}N_2O_2S_2$ $(M + H)^+$: 317.0418, Found: 317.0400.

Declaration of Competing Interest

The authors declare that they have no known competing financial interests or personal relationships that could have appeared to influence the work reported in this paper.

CRediT authorship contribution statement

Burak Kuzu: Data curation, Formal analysis, Methodology, Validation. **Sergen Gül:** Data curation, Formal analysis, Methodology, Validation. **Meltem Tan-Uygun:** Data curation, Formal analysis, Methodology, Validation. **Mesude Figen Dönmez:** Data curation, Formal analysis, Methodology, Validation. **Nurettin Menges:** Conceptualization, Project administration, Resources, Funding acquisition, Supervision, Writing – original draft, Writing – review & editing.

Data Availability

Supporting information files will be available

Acknowledgements

The Foundation from The Scientific and Technological Research Agency of Turkey (TÜBİTAK) (grant number:115Z894) was highly appreciated. We have recorded all NMR and HRMS data at the Science and Application Center of Van YYÜ, so the authors thank to head of the center for their support. The authors thank graphic designer Gül Menges for preparing the graphical abstract. N.M. thanks Turkish Academy of Sciences for financial support (TÜBA-GEBİP2019)

Supplementary materials

Supplementary material associated with this article can be found, in the online version, at doi:10.1016/j.molstruc.2022.134311.

References

[1] G. Achermann, T.M. Ballard, F. Blasco, P.-E. Broutin, B. Büttelmann, H. Fischer, M. Graf, M.-C. Hernandez, P. Hilty, F. Knoflach, A. Koblet, H. Knust, A. Kurt, J.R. Martin, R. Masciadri, R.H.P. Porter, H. Stadler, A.W. Thomas, J. Wichmann, Bioorg. Med. Chem. Lett. 19 (2009) 5746.
[2] B.A. Johns, J.G. Weatherhead, Y. Aoyama, H. Yoshida, Y. Taoda, Patent No: US 8, 691, 823, 2014
[3] [a] J.-C. Andrez, Beilstein J. Org. Chem. 5 (33) (2009) 1–36; [b] N. Chen, X. Meng, F. Zhu, J. Cheng, X. Shao, Z. Li, J. Agric. Food. Chem. 63 (5) (2015) 1360–1369.
[4] [4a] N.H. Metwally, M.A. Abdallah, S.A. Almabrook, J. Heterocyclic Chem., 54 (2017) 347–354; [4b] F.A. El-Essawy, Synt. Commun. 40 (2010) 877–887; [4c] S.N. Sirakanyan, D. Spinelli, A. Geronikaki, A.A. Hovakimyan, A.S. Noravyan, Tetrahedron 70 (2014) 8648–8656.
[5] [a] A. Maleki, M. Aghaei, Ultrason. Sonichem., 38 (2017) 585–589; [b] G.-You Lin, C.-Wen Li, S.-Hua Hung, R.-Shung Liu, Org. Lett. 10 (2008) 5059–5062.
[6] [a] E.C. Vatansever, K. Kilic, M.S. Özer, G. Koza, N. Menges, Tet. Lett. 56 (2015) 5386–5389; [b] B. Kuzu, H. Genc, M. Taspinar, M. Tan, N. Menges, Heteroatom Chem. 29 (2018) e21412; [c] D. Güçlü, B. Kuzu, İ. Tozlu, F. Taşpınar, H. Canpınar, M. Taşpınar, N. Menges, Bioorg. Med. Chem. Lett. 28 (2018) 2647–2651; [d] V. Tasdemir, N. Menges, Asian J. Org. Chem. 9 (2020) 2108–2111.
[7] V. Taşdemir, B. Kuzu, M. Tan, H. Genç, N. Menges, Synlett 30 (2019) 307–310.
[8] CCDC 1948493 contain the supplementary crystallographic data for this paper. These data can be obtained free of charge via www.ccdc.cam.ac.uk/data_request/cif, or by emailing data_request@ccdc.cam.ac.uk, or by contacting The Cambridge Crystallographic Data Centre, 12 Union Road, Cambridge CB2 1EZ, UK; fax: +44 1223 336033
[9] E.E. Kwan, Y. Zeng, H.A. Besser, E.N. Jacobsen, Nat Chem 10 (9) (2018) 917–923.
[10] O. Sari, A.F. Seybek, S. Kaya, N. Menges, S.S. Erdem, M. Balci, Euro. J. Org. Chem. (2019) 5261–5274.
[11] J.E. Baldwin, J. Chem. Soc. Chem Commun. 18 (1976) 734–736.
[12] [a] V. Schirch, D.M.E Szebenyi, 2005 Curr. Opin. Chem. Biol., 9 482–487; [b] T. Soderberg, Organic Chemistry with a Biological Emphasis Volume I, Chemistry Publications, 2019.
[13] [a] S. Saranya, R. Ramesh, J.G. Malecki, Euro. J. Org. Chem. 65 (2017) 6726–6733; [b] P. M.-Arvela, I.L. Simakova, D.Y. Murzin, Catal. Rev. (2021) in pressDOI, doi:10.1080/01614940.2021.1942689.
[14] S.M. Lee, A.H.S. Azizan, E.R.T. Tiekink, Molbank 4 (2018) 1–7.
[15] [a] A. Shaabani, M.T. Nazeri, R. Afshari, Mol. Divers. 23 (2019) 751; [b] W. Hu, W. Yang, T. Gang, W. Zhem, Y. Zheng, CrystEngComm. 21 (2019) 6630; [c] T. Hata, Y. Hayashi, Y. Hasegawa, M. Iwai, A. Ishii, M. Hasegawa, M. Shigeta, H. Urabe, Chem. Lett. 48 (2019) 662; [d] B. R: Raju, S. Naik, P.J.G. Coutinho, M.S.T. Gonçalves, Dyes Pigments 99 (2013) 220; [e] E.MS. Costanheira, M.S.D. Carvalho, A.R.O. Rodrigues, R.C. Colhelha, M.-Joao RP. Queiroz, Nanoscale Res. Lett. 6 (2011) 379; [f] B. Banerji, S. Chatterjee, K. Chandrasekhar, S. Ghosh, K. Mukherjee, C. Mandal, J. Org. Chem. 83 (2018) 13011.
[16] M.J. Frisch, G.W. Trucks, H.B. Schlegel, G.E. Scuseria, M.A. Robb, J.R. Cheeseman, G. Scalmani, V. Barone, B. Mennucci, G.A. Petersson, H. Nakatsuji, M. Caricato, X. Li, H.P. Hratchian, A.F. Izmaylov, J. Bloino, G. Zheng, J.L. Sonnenberg, M. Hada, M. Ehara, K. Toyota, R. Fukuda, J. Hasegawa, M. Ishida, T. Nakajima, Y. Honda, O. Kitao, H. Nakai, T. Vreven, J.A. Montgomery Jr., J.E. Peralta, F. Ogliaro, M. Bearpark, J.J. Heyd, E. Brothers, K.N. Kudin, V.N. Staroverov, R. Kobayashi, J. Normand, K. Raghavachari, A. Rendell, J.C. Burant, S.S. Iyengar, J. Tomasi, M. Cossi, N. Rega, J.M. Millam, M. Klene, J.E. Knox, J.B. Cross, V. Bakken, C. Adamo, J. Jaramillo, R. Gomperts, R.E. Stratmann, O. Yazyev, A.J. Austin, R. Cammi, C. Pomelli, J.W. Ochterski, R.L. Martin, K. Morokuma, V.G. Zakrzewski, G.A. Voth, P. Salvador, J.J. Dannenberg, S. Dapprich, A.D. Daniels, Ö. Farkas, J.B. Foresman, J.V. Ortiz, J. Cioslowski, D.J. Fox, Gaussian 09, Revision D. 01, Gaussian Inc, Wallingford CT, 2009, doi:10.1159/000348293.
[17] Ramprasad Misra, S.P. Bhattacharyy, Intramolecular Charge Transfer Theory and Applications, Wiley, Germany, 2018.
[18] [a] D.E. Brodersen, W.M. Clemons Jr, A.P. Carter, R.J. Morgan-Warren, B.T. Wimberly, V. Ramakrishnan, Cell 103 (2000) 1143–1154; [b] W. Hinrichs, C. Kisker, M. Düvel, A. Müller, K. Tovar, W. Hillen, W. Saenger, Science 264 (1994) 418–420.